Author Manuscript

Title: Ultra-Permeable Dual-Mechanism-Driven Graphene Oxide Framework Membranes for Precision Ion Separations

Authors: Jing Guo; Yanqiu Zhang; Fan Yang; Bhekie B. B. Mamba; Jun Ma; Lu Shao; Shaomin Liu, PhD

To be cited as: 10.1002/anie.202302931

Link to VoR: https://doi.org/10.1002/anie.202302931

WILEY-VCH

RESEARCH ARTICLE

Ultra-Permeable Dual-Mechanism-Driven Graphene Oxide Framework Membranes for Precision Ion Separations

Jing Guo[a], Yanqiu Zhang[a,b], Fan Yang[a], Bhekie B. Mamba[c], Jun Ma[b], Lu Shao*[a] and Shaomin Liu*[d]

[a] J. Guo, Y. Zhang, F. Yang, L. Shao
MIIT Key Laboratory of Critical Materials Technology for New Energy Conversion and Storage, State Key Laboratory of Urban Water Resource and Environment (SKLUWRE), School of Chemistry and Chemical Engineering
Harbin Institute of Technology
Harbin 150001, China
E-mail: shaolu@hit.edu.cn

[b] Y. Zhang, J. Ma
State Key Laboratory of Urban Water Resource and Environment (SKLUWRE), School of Environment
Harbin Institute of Technology
Harbin 150090, China

[c] B. B. Mamba
Institute for Nanotechnology and Water Sustainability, College of Engineering, Science and Technology
University of South Africa, Florida Science Campus
1709 Roodepoort, South Africa

[d] S. Liu
WA School of Mines: Minerals, Energy and Chemical Engineering
Curtin University
WA, Australia
E-mail: shaomin.liu@curtin.edu.au

Supporting information for this article is given via a link at the end of the document.

Abstract: Two-dimensional graphene oxide (GO) membranes are gaining popularity as a promising means to address global water scarcity. However, current GO membranes fail to sufficiently exclude angstrom-sized ions from solution. Herein, a de novo "posterior" interfacial polymerization (p-IP) strategy is reported to construct a tailor-made polyamide (PA) network in situ in an ultrathin GO membrane to strengthen size exclusion while imparting a positively charged membrane surface to repel metal ions. The electrostatic repulsion toward metal ions, coupled with the reinforced size exclusion, synergistically drives the high-efficiency metal ion separation through the synthesized positively charged GO framework (PC-GOF) membrane. This dual-mechanism-driven PC-GOF membrane exhibits superior metal ion rejection, anti-fouling ability, good operational stability, and ultra-high permeance (five times that of pristine GO membranes), enabling a sound step towards a sustainable water–energy–food nexus.

Introduction

Water scarcity and water resource pollution are serious threats to global sustainable development and have been particularly escalated by climate change and the COVID-19 pandemic when considering the fragile state of the water–energy–food nexus.[1–3] According to the Sustainable Development Goals Report 2022, 2 billion people worldwide do not have access to healthy drinking water. Therefore, the development of energy-efficient water purification with high efficiency and wastewater recycling technologies is critical.[4,5] Membrane separation technology, characterized by its low energy consumption, zero secondary pollutant emissions, low carbon footprint, and high design flexibility, has the potential to become the mainstream method for water purification and alleviate issues pertaining to water resources.[6,7] Prior to the realization of this potential, the development of novel membranes with upgraded separation performance for lower cost and higher output is necessary but still challenging.[8–10]

Two-dimensional (2D) membranes fabricated from atom-thick nanosheets exhibit unprecedented separation properties owing to their highly ordered 2D nanofluidic channels for separation.[11–13] For instance, 2D graphene oxide (GO) membranes display outstanding water permeability owing to their high in-plane porosity and interlamellar nanochannels for ultrafast water molecule permeation.[14–16] Nonetheless, the separation of ions, particularly the removal of metal ions that are detrimental to human health, by GO-based membranes encounters extreme challenges. It is well known that membrane-based separations of ions in solution depend mainly on the size-sieving effect and electrostatic interactions. However, ionic dissociation of oxygen-containing groups on GO nanosheets imparts a negatively charged surface, causing failure of GO membranes to repel metal ions in terms of electrostatic interactions.[17,18] On the other hand, abundant oxygen-containing groups endow GO nanosheets with excellent hydrophilicity, which, in conjunction with the mutual electrostatic repulsion between negatively charged GO nanosheets, leads to unfavorable swelling and enlargement of the interlayer *d*-spacing of GO membranes upon exposure to an aqueous environment.[19] The swelling not only diminishes the size exclusion capability of the membrane toward angstrom-sized metal ions,[20] but also overwhelmingly jeopardizes the robustness of the GO membranes for practical applications.[21,22] Although several protocols have been reported for the confinement of the interlayer *d*-spacing of GO membranes, including chemical reduction,[23] chemical crosslinking,[24–26] and physical confinement,[27] precisely regulating the interlayer channels of

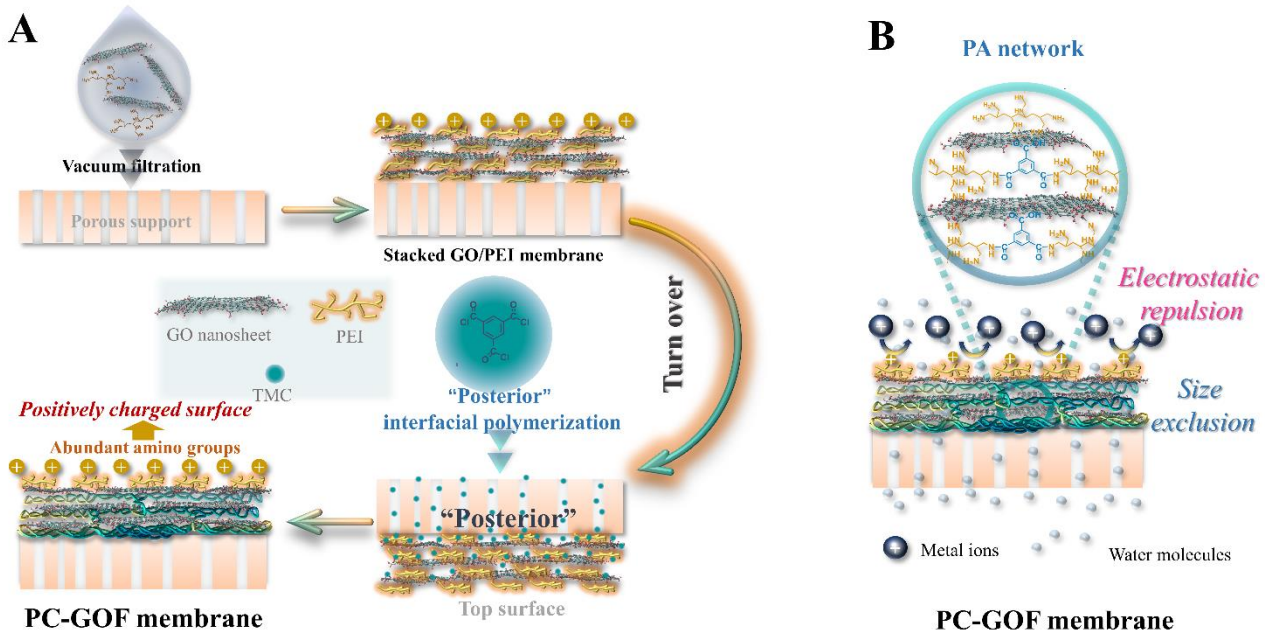

Figure 1. Scheme describing the fabrication and ion separation mechanism of the PC-GOF membrane. (A) Fabrication of the PC-GOF membrane via the p-IP technique. (B) Ion separation of the PC-GOF membrane via the cooperative effect of size exclusion and electrostatic repulsion.

laminated GO membranes for high-efficiency ion separation in practical pressure-driven filtration process is still technologically challenging.[28] Moreover, decreasing hydrophilicity by reduction or constricting GO nanochannels via chemical or physical confinement will sharply slow the mass transport, and thus, it will sacrifice the membrane permeability.[29–31]

Recently, integrating other separation-functional architectures into 2D GO membranes to synergistically exploit individual advantages has offered a new platform for the manufacturing of high-efficiency separation membranes.[32–34] As the major separating component of commercial reverse osmosis (RO) or nanofiltration (NF) membranes, selective polyamide (PA) films fabricated via interfacial polymerization (IP) feature high retention of salt ions.[35,36] Constructing PA networks in GO membranes can enhance the size-sieving capacity to block solutes. However, in terms of electrostatic interactions, the negative ionization of conventional PA networks in water plays an adverse role when deploying PA-based membranes to exclude metal ions. [37–40] Accordingly, importing PA networks into GO membranes for the desirable retention of metal ions necessitates a dense PA network to impart a sufficient size-sieving effect, which inevitably generates tremendous mass-transfer resistance and sharply compromises the membrane permeability.

Herein, we develop a de novo "posterior" interfacial polymerization (p-IP) technique to construct a positively charged GO framework (PC-GOF) membrane for high-efficiency ion separations. By regulating the IP process, specifically controlling the diffusion of monomers in a laminated GO film, a tailor-made PA network was constructed in situ in the GO membrane, and at the same time, a highly positively charged surface of the resultant GO framework membrane was obtained. Polyethyleneimine (PEI) as an aqueous phase monomer was previously immobilized onto laminated GO nanosheets by incorporation to form a positively charged GO/PEI film. The organic phase monomer trimesoyl chloride (TMC) was introduced from the backside ("posterior") of the GO/PEI film to crosslink with the PEI molecules, constructing a PA network in situ in the GO laminate. As the diffusion of TMC was regulated to occur from the bottom to the top surface of the laminated GO/PEI film, abundant amino groups from PEI molecules on the top surface could be preserved, affording a positively charged surface and outstanding hydrophilicity of the PC-GOF membrane (Figure 1A). The electrostatic repulsion of metal ions triggered by the positively charged surface, in conjunction with the improvement of the size-sieving effect from the incorporated PA network, endowed the PC-GOF membrane with high-efficiency separation of metal ions (Figure. 1B). Moreover, assisted by the electrostatic repulsion of metal ions from the positively charged membrane surface, the superiorly permeable PC-GOF membrane exhibited surpassing metal ion retention compared to the nascent GO membrane, indicating a breakthrough in the permeability-selectivity trade-off. In addition, the remarkable surface hydrophilicity endowed the PC-GOF membrane with excellent antifouling performance, and the p-IP-formed PA network conferred desirable ultrastability.

Results and Discussion

Morphologies and chemical structures of the synthesized PC-GOF membranes.

A microporous polyethersulfone (PES) membrane (Supplementary Figure S1) was used as a support for the fabrication of GO-based membranes, and atom-thick GO nanosheets with small lateral sizes (Supplementary Figure S2) were synthesized to access the GO-based membranes. The GO

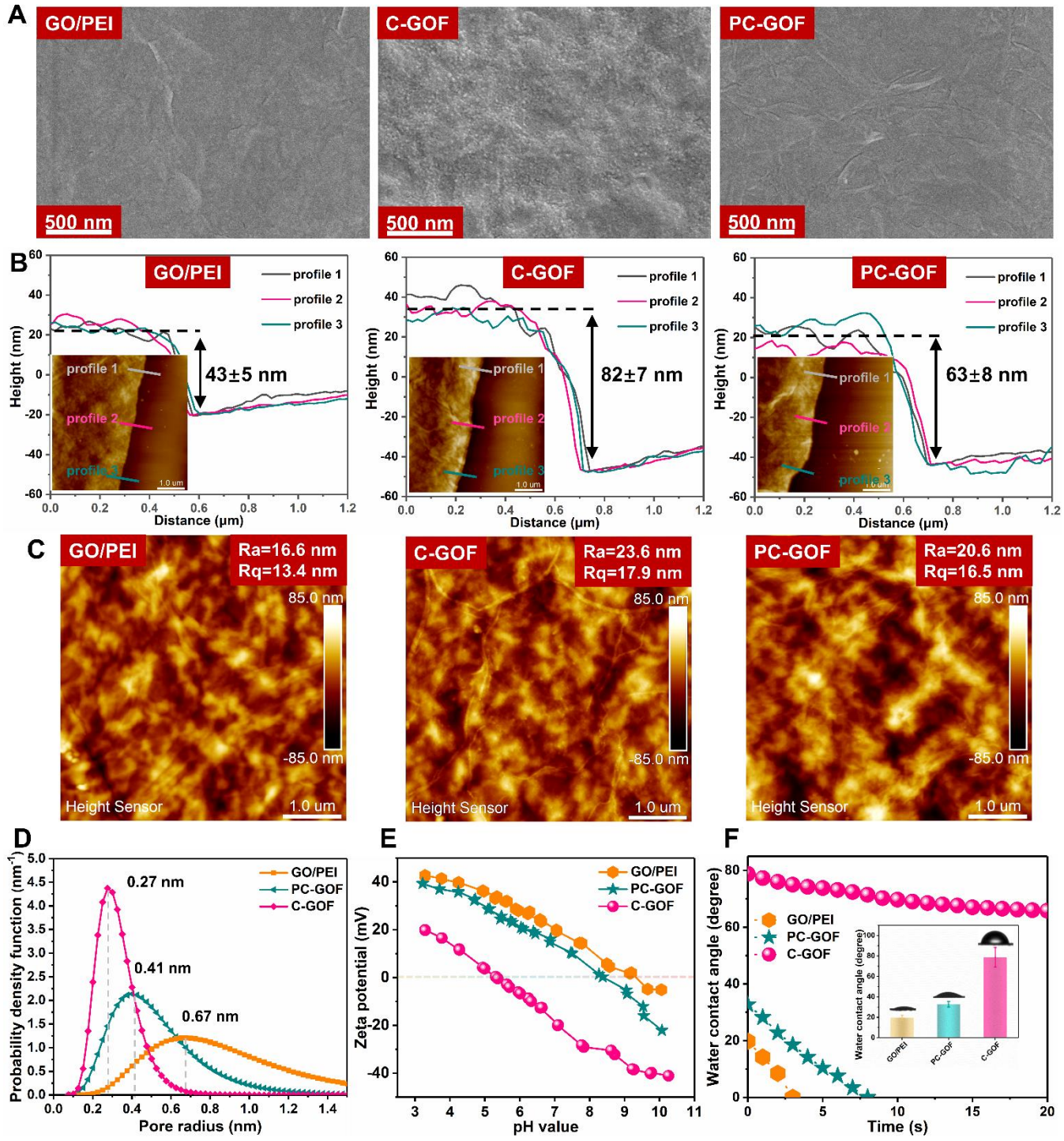

Figure 2. Structures and properties of the as-prepared GO-based membranes. (A) Top and (B) cross-sectional SEM images of GO/PEI, C-GOF, and PC-GOF membranes. (C) AFM images and roughness of GO/PEI, C-GOF, and PC-GOF membranes. (D) Pore size distribution curves, (E) zeta potentials and (F) dynamic water contact angles of the as-prepared GO/PEI, PC-GOF, and C-GOF membranes (inset: initial water contact angles of the GO/PEI, PC-GOF, and C-GOF membranes)

suspension was slowly added to PEI solutions to form a homogeneous dispersion. Then, the mixture of GO and PEI was filtered through the PES support, and a uniform GO/PEI membrane was obtained (Supplementary Figure S3). The PC-GOF membrane was then obtained by performing a p-IP process on the "posterior" of the GO/PEI membrane. To highlight the merits of the p-IP strategy, we also created a GO framework membrane using a traditional IP procedure and named it the C-GOF membrane. The top and cross-sectional morphologies of the as-prepared GO-based membranes were examined using scanning electron microscopy (SEM), transmission electron microscopy (TEM) and atomic force microscopy (AFM). The GO/PEI membrane fabricated via a vacuum-assisted filtration process exhibits a defect-free and 43 ± 5 nm laminated selective film (Figure 2A and B, Supplementary Figure S4),[41] in which GO

nanosheets were parallelly arranged and presented a typical layered structure (Supplementary Figure S5). The selective film of the C-GOF membrane was significantly thicker (approximately 82 nm) than that of the GO/PEI membrane, and abundant nanosized PA nodules emerged on the top surface of the C-GOF membrane, causing a rougher surface (Figure 2C). The thicker selective film and emerging nodules on the surface of the C-GOF membrane demonstrate the formation of a PA network via the crosslinking reaction between PEI and TMC molecules.[42,43] After the p-IP process, the acquired PC-GOF membrane also revealed a layered skeleton in the GO-based selective film (Supplementary Figure S6). The selective layer of the PC-GOF membrane has a thickness of approximately 63 nm, which is a 20 nm increase compared to that of the GO/PEI membrane. The thicker selective layer of the PC-GOF membrane compared to the GO/PEI membrane should be ascribed to the formation of the PA network, which could be verified by the nodule-like structures observed at the backside of the PC-GOF selective layer (Supplementary Figure S7). Interestingly, no obvious nodule-like structures were identified on the PC-GOF membrane surface, which indicated PEI molecules on the top surface did not participate in the crosslinking reaction with TMC during the p-IP process; consequently, an abundant amount of the amino groups on the membrane surface should be preserved.

In addition, fully reflected infrared (ATR-IR) spectroscopy and X-ray photoelectron spectroscopy (XPS) were utilized to probe their chemical structures and IP reaction during the membrane fabrication process. The N–H peak at 3300–3500 cm^{-1} in the ATR-IR spectrum of the GO/PEI membrane (Supplementary Figure S8) and the appearance of a new N 1s peak in the XPS spectrum of the GO/PEI membrane (Supplementary Figure S9 and Table S1) indicated the existence of abundant amino groups, which originated from the intercalation of PEI molecules into the GO laminate. After the conventional IP process, peaks attributed to the C=O stretch of amide group I (at approximately 1660 cm^{-1}) and C–N of amide group II (at approximately 1546 cm^{-1}) were observed in the ATR-IR spectra of the PC-GOF and C-GOF membranes, indicating the formation of the PA network in these membranes.[44] Construction of the PA network in the laminated GO/PEI film apparently reinforced the size exclusion effect toward solute (Figure 2D), as evidenced by the narrower pore size of the PC-GOF (mean pore radius of 0.41 nm) and C-GOF (mean pore radius of 0.27 nm) membrane than that of the pristine GO/PEI membrane (mean pore radius of 0.67 nm). In addition, the wider pore size of the PC-GOF membrane demonstrated that the PA network constructed via the p-IP strategy is looser than that in the C-GOF membrane. This looser PA network in the PC-GOF membrane should be ascribed to the lower density of PEI molecules on the rear surface, which was revealed by the higher O/N ratio of the rear surface (Supplementary Figure S10). We speculate that PEI molecules were gradually concentrated during the fabrication process of the GO/PEI film via a filtration process. Hence, the concentration of PEI molecules on the top surface was higher than that on the rear surface, which resulted in a denser PA network in the C-GOF membrane as PEI molecules with a higher concentration participated in the crosslinking reaction in a conventional IP process. The weaker ATR-IR peaks of amide groups (Supplementary Figure S8), assisted by the lower content of amide groups observed in the narrow C 1s spectrum of the PC-GOF membrane (Supplementary Figure S11),[45,46] verified that the PA network constructed in the PC-GOF membrane was looser than that in the C-GOF membrane. The looser PA network in the PC-GOF membrane represents lower mass-transport resistance and thus should correspond to higher permeance than the C-GOF membrane. In addition, a new peak attributed to the C–O stretch of the carboxyl group emerged in the ATR-IR spectrum of the C-GOF membrane, indicating that some residual acyl chloride groups from the TMC molecules hydrolyzed into carboxyl groups during the conventional IP process. These carboxyl groups commonly endow the formed PA layer with a negatively charged surface. By contrast, the C–O stretch is unapparent in the ATR-IR spectrum of the PC-GOF membrane, which in conjunction with the higher content of amine groups observed in the high-resolution N 1s XPS spectrum of the PC-GOF membrane (Supplementary Figure S12) further verified that the p-IP strategy reserved many amino groups on the surface of the PC-GOF membrane.

The difference in the surface chemical structure of different GO framework membranes will affect the properties of the membrane surface, especially the surface charge properties and hydrophilicity, which are significant to membrane separation performance. The positive value of the zeta potential of the GO/PEI membrane revealed that the intercalation of PEI molecules transformed the negatively charged surface of the GO membrane into a positively charged surface (Figure 2E and Supplementary Figure S13). By contrast, the positively charged property of the GO/PEI membrane reversed under conventional IP because the amino groups on the top surface were consumed and the residual acyl chloride groups of TMC were hydrolyzed into carboxyl groups. The negatively charged surfaces of the GO and C-GOF membranes cannot repel metal ions via electrostatic repulsion. In terms of the zeta potentials of the PC-GOF membrane, as the IP reaction occurred near the backside of the GO/PEI film and the PEI molecules on the top surface avoided consumption, the PC-GOF membrane exhibited a positive zeta potential, indicating a positively charged surface. This will facilitate the rejection of positively charged ions, particularly multivalent metal ions, by the PC-GOF membrane. In addition, the GO framework membranes fabricated via different IP strategies exhibited different hydrophilicity (Figure 2F). The initial water contact angle of the pure GO membrane was approximately 65° and dropped to 0° after 13 s (Supplementary Figure S14). Owing to the abundant hydrophilic amino groups on the top surface, the GO/PEI membrane exhibited a much lower water contact angle of 19.8°, which rapidly dropped to 0° within 3 s, indicating excellent hydrophilicity. After the conventional IP process, the initial water contact angle of the fabricated C-GOF membrane increased to 78.8°, which slowly declined to approximately 68.1° after 20 s. The much higher water contact angle of the C-GOF membrane was ascribed to the consumption of hydrophilic PEI molecules on the top surface during conventional IP. In addition, the absence of PEI molecules coupled with the dense PA network formed on the C-GOF membrane surface hindered the fast permeation of water molecules, thus resulting in a much slower decrease in the water contact angles. In comparison, as a result of the preservation of hydrophilic amino groups on the top surface, the PC-GOF membrane exhibited an initial water contact angle of approximately 32.7°, which decreased rapidly with time, indicating a prominent hydrophilic surface.

Manipulation of p-IP technique for membrane fabrication.

To gain insight into the construction of the PA network occurring during the p-IP process, the effect of the reaction time on the

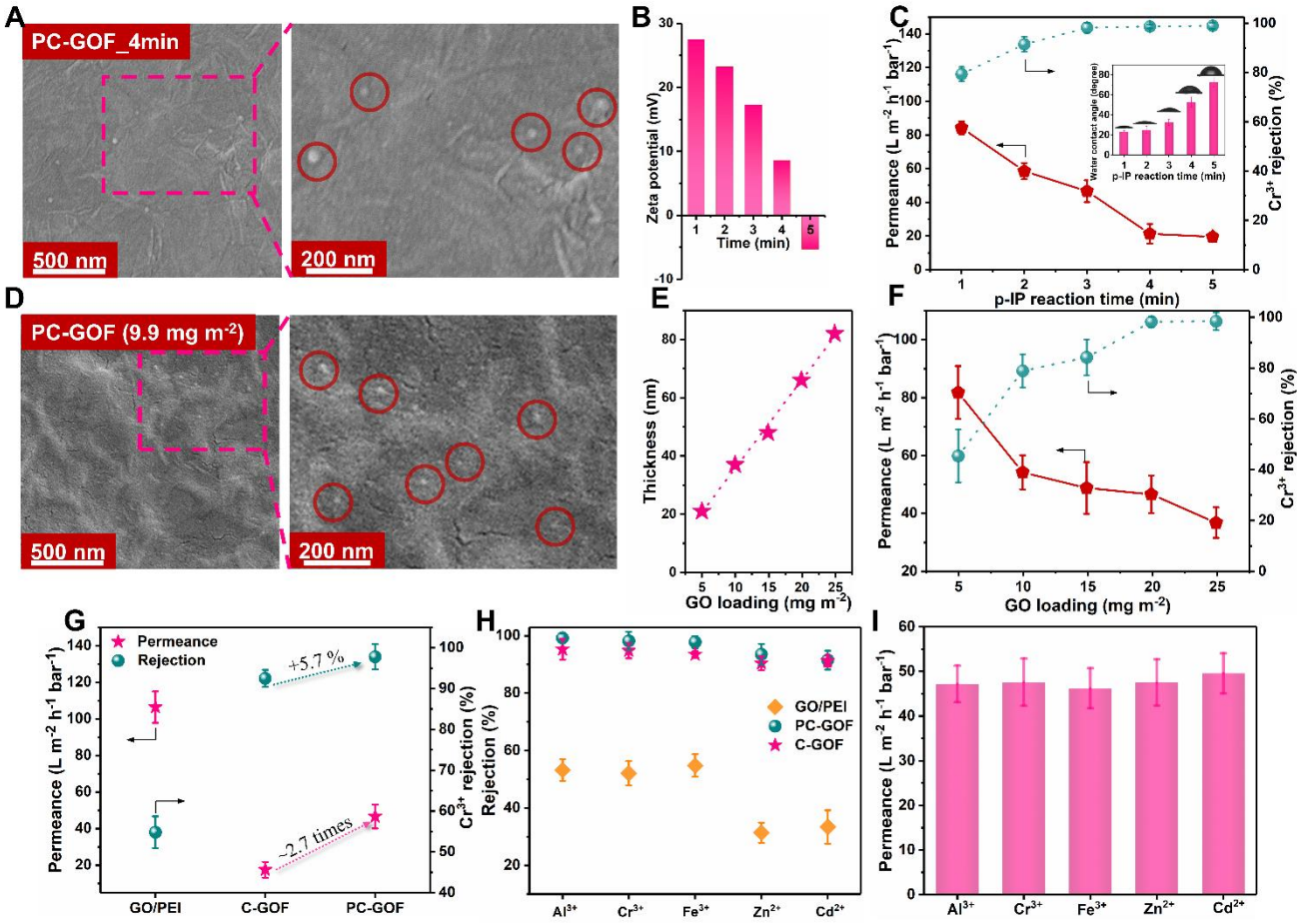

Figure 3. Investigation of the p-IP technique on the properties and performance of PC-GOF membranes. (A) Top-view SEM image of the PC-GOF membrane with a p-IP reaction time of 4 min. (B) Zeta potentials of PC-GOF membranes at about pH 7 with different p-IP reaction time. (C) Variation in the ion separation performance of PC-GOF membranes with increasing p-IP reaction time (inset: water contact angles of PC-GOF membranes with different p-IP reaction time). (D) Top-view SEM image of the PC-GOF membranes with a GO loading of 9.9 mg m^{-2}. (E) Thickness of PC-GOF membranes as a function of GO loadings. (F) Permeance and Cr^{3+} rejection of PC-GOF membranes as a function of GO loading. (G) Permeance and Cr^{3+} rejection of the as-prepared GO-based membranes. (H) Rejections of different metal ions of as-prepared GO-based membranes. (I) Permeance of the PC-GOF membranes when filtering different salt solutions.

structure and separation performance of the as-prepared p-GO/PEI membranes were first studied. The PC-GOF membranes prepared with different reaction time exhibited a noticeable difference in their morphologies; when the reaction time increased, the roughness of the top surface of the PC-GOF membrane gradually appeared to increase with more wrinkles (Supplementary Figure S15). Notably, when the reaction time surpassed 4 min, nodule-like PA structures appeared on the PC-GOF_4min top surface (Figure 3A); a further increase in the reaction time led to the formation of additional nodule-like nanostructures (Supplementary Figure S16). This phenomenon indicates that some PA structures emerge at the top surface of the membranes and suggests that some TMC molecules diffused from the bottom to the top surface and reacted with PEI molecules on the top surface during the p-IP process for a sufficiently long diffusion time. The escalating intensity of the amide groups in the ATR-IR spectra (Supplementary Figure S17) and declining surface N content of the PC-GOF membranes (Supplementary Figure S18, Table S2) indicated that increased PEI molecules on the surface participated in the crosslinking reaction and were consumed with increasing p-IP reaction time. The increasing consumption of PEI molecules on the surface along with the increased reaction time results in decreasing zeta potential values (Figure 3B). Figure 3C indicates that the rejection of PC-GOF toward Cr^{3+} increased, and the pure water permeance of the membrane decreased with increasing p-IP reaction time. The increased Cr^{3+} rejection should be due to the reinforced size exclusion arising from the continuously growing PA network in the membrane. Meanwhile, the PA network enhanced the mass-transport resistance toward water molecules, which, in conjunction with the degressive hydrophilicity (Figure 3C), led to decreased water permeance. Notably, when p-IP was allowed to proceed for 3 min, the resultant PC-GOF membrane exhibited a high rejection rate of 98.2% toward Cr^{3+}; however, a longer reaction time failed to substantially enhance the rejection and instead led to a sharp decrease in the water permeance.

Furthermore, we investigated the influence of the GO nanosheet dosage on the PC-GOF membrane performance. Nodule-like PA structures formed on the surface of the PC-GOF membranes when the GO loading was sufficiently low (4.9 and 9.9 mg m^{-2}), while PA nodules did not appear on the surface of the PC-GOF (14.9 mg m^{-2}), PC-GOF (19.9 mg m^{-2}) and PC-GOF (24.9 mg m^{-2}) membranes (Figure 3D, Supplementary Figure S19). As a higher GO loading corresponds to a thicker GO/PEI laminated film (Supplementary Figure S20), the PA nodules on the top surface

of the PC-GOF membrane with a low GO loading demonstrate that TMC molecules can penetrated through a thin GO/PEI film and react with PEI molecules on the top surface to form PA structures, whereas a thicker GO/PEI film hinders the TMC molecules from reaching the top surface. Notably, the thickness of the selective layer of the PC-GOF membrane was almost linearly dependent on GO loadings (Figure 3E), while the separation performance of the PC-GOF membrane exhibited a nonlinear correlation with the GO loading (Figure 3F). This result reveals that the separation performance, particularly the permeability of the PC-GOF membrane, was not proportional to the selective layer thickness. The variation in the morphology and permeability of the PC-GOF membrane with different GO loadings indicated that the PA network was heterogeneously distributed in the vertical direction of the PC-GOF selective layer. This structural heterogeneity of the PA network was further directly disclosed by XPS characterizations. The O/N ratio of the PC-GOF membrane dropped from 2.10 to 1.21 when the GO loading increased from 4.9 mg m^{-2} to 24.9 mg m^{-2} (Supplementary Figure S21, Table S3). This phenomenon should be attributed to the diffusion of TMC molecules from the backside to the top surface of the GO/PEI film during a p-IP process. When the organic solution containing TMC was poured onto the back of the GO/PEI membrane, TMC molecules rapidly passed through the PES substrate and reached the backside of the GO/PEI film to react with PEI molecules; thus, a PA network first formed on the backside of the GO/PEI film. Thereafter, TMC molecules diffused into the interior of the GO/PEI film, forming the PA network in the interior of the thin GO/PEI film. TMC molecules were also consumed by the reaction with PEI molecules when they diffused from the backside to the top surface of a GO/PEI film. In addition, the formed PA network further impeded the diffusion of TMC molecules to the top surface of a GO/PEI film. Hence, the diffusion of TMC molecules was retarded and gradually stalled. The GO loading is higher, the GO/PEI film is thicker, and fewer TMC molecules can penetrate through the GO/PEI film to react with PEI molecules on the membrane surface. That is, less PA molecules were formed and more PEI molecules were reserved on the surface of a PC-GOF membrane with a higher GO loading. Accordingly, the PA network formed by the p-IP strategy was heterogeneously distributed in the PC-GOF membrane, and the mass-transfer resistance did not increase linearly, which resulted in a nonlinear correlation between the membrane thickness and water permeance. In addition, because the membrane with a GO loading of 19.9 mg m^{-2} and 66 nm thickness exhibited a rejection rate exceeding 98% with high water permeance, it was set as the benchmark for separation performance investigations.

Separation performance of PC-GOF membranes synthesized via the p-IP technique.

Figure 3G shows the comparison of the separation performance among the optimal PC-GOF membrane with the GO/PEI and C-GOF membranes. As the ultrathin selective layer, superior hydrophilicity of the GO/PEI membrane and the enlarged interlayer spacing of the GO laminate from approximately 8.2 Å of the pure GO membrane to 13.3 Å (Supplementary Figure S22), the GO/PEI membrane exhibited a high permeance of 105.6 L m^{-2} h^{-1} bar^{-1}. After the conventional IP reaction, although the interlayer spacing of the C-GOF membrane did not exhibit a prominent change, the formed dense PA network endowed the C-GOF membrane with a lower permeance of 17.5 L m^{-2} h^{-1} bar^{-1}, and Cr^{3+} rejection increased from <60% for the GO/PEI membrane to 92.5% for the C-GOF membrane. Interestingly, the PC-GOF membrane exhibited an unprecedented simultaneous enhancement of the water permeance and ion rejection compared to that of the C-GOF membrane, with a high permeance of 46.6 L m^{-2} h^{-1} bar^{-1}, an excellent rejection of more than 98% to $CrCl_3$ solution, and a pure water permeance of more than 60 L m^{-2} h^{-1} bar^{-1} (Supplementary Figure S23). The higher water permeance of the PC-GOF membrane compared to that of the C-GOF membrane was attributed to the lower mass-transport resistance originating from the looser PA network and superior hydrophilicity. Conversely, although the size exclusion of the PC-GOF membrane is weaker than that of the C-GOF membrane, the electrostatic repulsion generated by the positively charged top surface endows the PC-GOF membrane with a higher ion rejection toward positively charged metal ions. Consequently, not only did the PC-GOF membrane exhibit a high rejection toward metal ions owing to the synergistic effect of size exclusion and electrostatic repulsion, but it also offered excellent permeability, indicating superior water purification performance.

The performance of the as-prepared PC-GOF membrane for the treatment of wastewater was investigated. Both of the PC-GOF and C-GOF membranes exhibited enhanced rejection toward nanosized organic dyes compared with the GO/PEI and the blank GO membrane (Supplementary Figures S24 and S25). Notably, the retentate dye solution was concentrated after filtration tests (Supplementary Figures S26). In addition, the adsorption of dyes on the PC-GOF membrane is slight with all of the adsorption percentage of the PC-GOF membrane when filtrating various dyes is below 10% (Supplementary Figures S27–S28), which is inconspicuous when compared to the high dye rejection. Therefore, the higher retention toward organic pollutants demonstrates that the PA network in the PC-GOF membrane imparted an improvement in size-sieving capacity. The higher rejection of the PC-GOF membrane toward dyes indicated that the PC-GOF membrane exhibited superior performance not only in ion separations but also in the removal of organic pollutants. For the retention of angstrom-sized metal ions, the rejection toward different metal ions by the PC-GOF membrane was higher than that by the C-GOF membrane; the evaluated rejection by the PC-GOF membrane toward different metal ions was in the order Al^{3+} (99.2%) > Cr^{3+} (98.2%) > Fe^{3+} (97.8%) > Zn^{2+} (93.6%) > Cd^{2+} (91.5%) (Figure 3H). The permeance of the PC-GOF membrane for solutions containing the above ions exceeded 45 L m^{-2} h^{-1} bar^{-1} (Figure 3I). We also evaluated the rejections of the PC-GOF membrane toward alkali and alkaline earth metal ions, and the rejections follow the order Mg^{2+} (90.3%) > Ca^{2+} (81.6%) > Na^{+} (15.6%) > K^{+}(15.9%) Owing to the electrostatic repulsion, the rejection of the PC-GOF membrane toward metal ions with a trivalent or divalent prominently surpasses the rejection toward monovalent alkali metal ions.[47] In addition, the rejection toward ions of the same valence was positively correlated to the hydrated ion radius.[48]

Profiting from its prominently enlarged interlayer spacing and ingeniously tailored PA network, the PC-GOF membrane in this work exhibited approximately five times the permeance of the GO membrane, and the electrostatic effect coupled with the size-sieving PA network endowed the PC-GOF membrane with an approximately 19.5% metal ion-rejection rate (Figure 4A), resulting in an outstanding performance that overcomes the trade-off between permeability and selectivity. In addition, upon comparing the performance with reported 2D or other novel

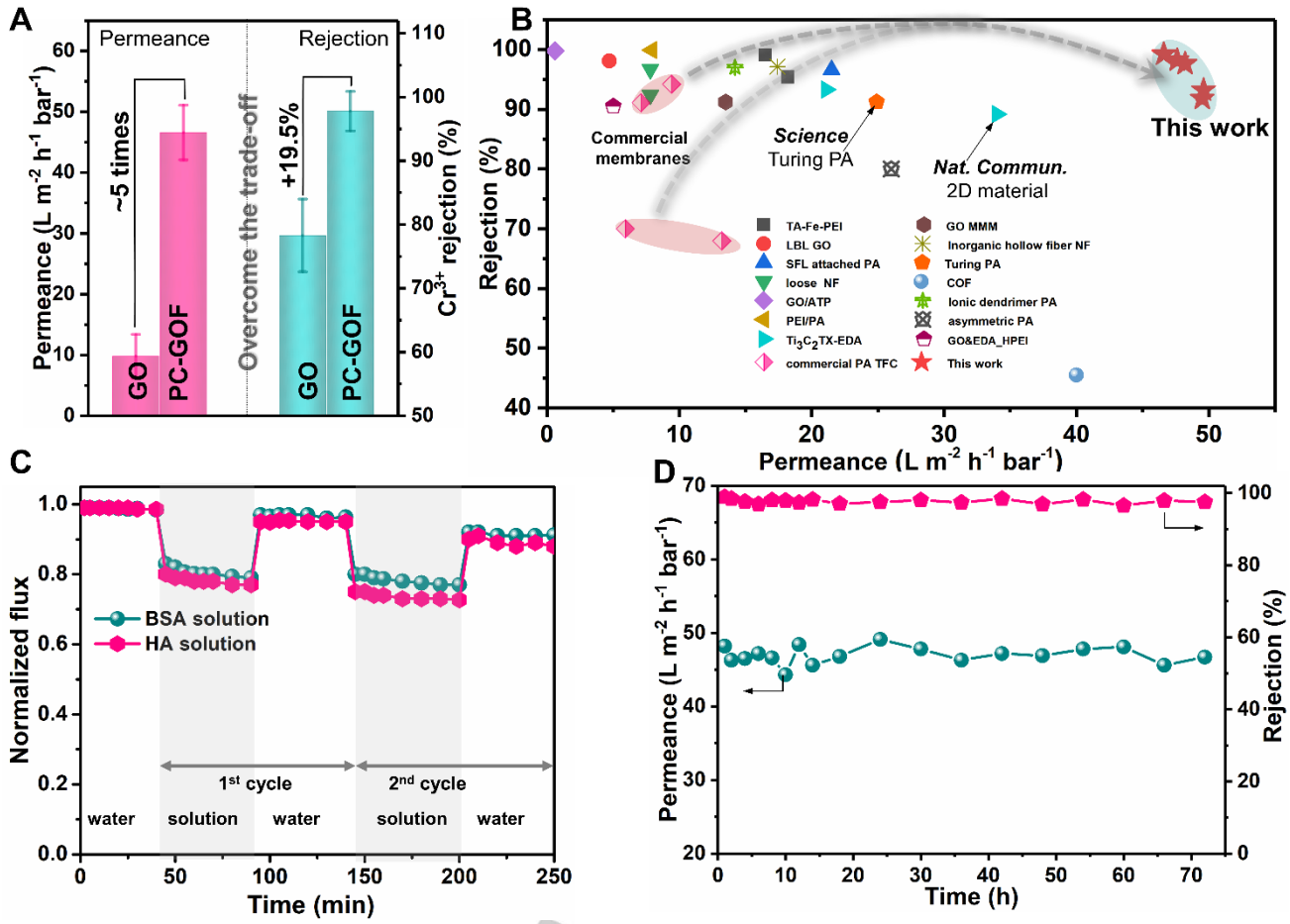

Figure 4. Ion separation performance of the PC-GOF membrane. (A) Comparison of the ion-separation performance between the blank GO and PC-GOF membranes. (B) Comparison of the ion-separation performance of the PC-GOF membrane with reported state-of-the-art membranes. (C) Normalized flux of permeance of the PC-GOF membrane in the fouling–cleaning filtration tests. (D) Permeance and Cr^{3+} rejection of the PC-GOF membrane in a continuous long-term test.

membranes for the separation of aqueous solutions containing metal ions, the prepared PC-GOF membrane exhibited superiority to state-of-the-art membranes and prominently promoted metal ion separation performance (Figure 4B, Supplementary Table S4).

Membrane fouling is another challenge in separation applications and has the potential to derail the long-term usage of membranes. Therefore, the antifouling performance of the as-prepared PC-GOF membrane was investigated by conducting fouling tests. The flux of the PC-GOF membrane decreased in the presence of the model foulants (BSA and HA) but rapidly recovered after washing (Figure 4C), indicating low irreversible fouling and a higher flux recovery ratio (FRR) value (Supplementary Figure S30). Owing to its superior hydrophilicity, the as-prepared PC-GOF membrane exhibited excellent antifouling performance. After two fouling cycles, approximately 90% pure water flux of the PC-GOF membrane was maintained, and the calculated FRR of the PC-GOF membrane was found to be 96.3% (BSA) and 94.8% (HA) during the first fouling cycle and 91.2% (BSA) and 90.2% (HA) for the second fouling cycle. In addition, the PC-GOF membrane maintained a stable separation performance, with a permeance of over 45 L m^{-2} h^{-1} bar^{-1} and a Cr^{3+} rejection rate of 97%, which was achieved in a 72-hour continuous test (Figure 4D). Especially, compared to the drastic decline of permeance from about 65 L m^{-2} h^{-1} bar^{-1} to below 10 L m^{-2} h^{-1} bar^{-1} of the blank GO membrane (Supplementary Figure S31), the PC-GOF membrane only exhibited a slight decrease in permeance. We attributed this distinction in permeance stability to the incorporation of PA networks in the GO laminate. GO membranes were extremely compacted under long-term pressure filtration, and the compaction of interlayer channels of GO membranes resulted in a sharp decline of permeability.[49] When the pressure was deployed on the PC-GOF membrane, the PA networks immobilized the laminated GO nanosheets and resisted the compaction.

Poor hydraulic stability is one of the GO-based membranes, and the prepared PC-GOF membrane was vigorously sonicated in water to evaluate the membrane robustness. Upon strong sonication, some GO nanosheets exfoliated from the GO/PEI membrane and damaged the integrity of this membrane (Supplementary Figure S32). By contrast, the macroscopic and microscopic characterization of the PC-GOF membrane morphology revealed that no delamination of GO nanosheets or morphological defects were observed after the drastic sonication test, indicating good structural stability of the PC-GOF membrane. The superior robustness of the PC-GOF membrane should be first ascribed to the interlocking of the GO nanosheets by the integrated PA network, which builds up a robust covalent bridging

network throughout the GO laminate to tightly immobilize GO nanosheets and avoid delamination.[50] In addition, residual PEI molecules in the pores of the PES substrate of the GO/PEI membrane reacted with TMC molecules during the p-IP process and formed PA structures in the pores of the PES support of the PC-GOF membrane (Supplementary Figures S33). Some PA structures in the pores of the PES support were integrated into the PA network in the PC-GOF selective film and imparted an anchoring effect at the interface between the PC-GOF selective film and the substrate, avoiding the exfoliation of GO laminates from the PES support (Supplementary Figure S34). The anchoring effect from the PA structures in the interface, in conjunction with the interlocking effect from the PA network in GO laminates, endowed the PC-GOF membrane with high structural robustness, which assured the long-term stability of the PC-GOF membrane in a practical water purification process.

Conclusion

The novel p-IP strategy proposed in this study was validated as effective in the construction of highly positively charged GO framework membranes for high-efficiency metal ion separations. The two-pronged promotion towards membrane selectivity, the reinforced size exclusion that stemmed from the integrated PA network and the electrostatic repulsion that resulted from the positively charged surface of the PC-GOF membrane endowed this membrane with metal ion separation performance that outperformed the reported state-of-the-art membranes. In addition, compared to conventional IP technology, the p-IP strategy not only endowed the PC-GOF membrane with superior permeance by forming a less-mass-transport-resistant looser PA network but also afforded superior selectivity toward metal ions by the cooperative effect of electrostatic repulsion and size exclusion. Furthermore, the excellent hydrophilicity imparted by the abundant amino groups on the membrane surface conferred excellent anti-fouling capability, and the incorporated PA network contributed ultra-stability to the PC-GOF membrane. The de novo p-IP strategy implemented in this work can be adopted and expanded to other 2D materials and integrated into next-generation membranes for high-efficiency water purification applications.

Acknowledgements

This work was financially supported by the National Natural Science Foundation of China (22178076, 22208072), the Natural Science Foundation of Heilongjiang Province for Distinguished Young Scholars (JQ2020B001), Heilongjiang Touyan Team (HITTY-20190033), Fundamental Research Funds from the Central Universities of Ministry of Education of China and State Key Laboratory of Urban Water Resource and Environment (Harbin Institute of Technology) (No. 2020DX02) and the Australian Research Council (DP180103861 and IH170100009).

Keywords: membranes • graphene • “posterior” interfacial polymerization • water treatment • positively charged surface

[1] K. Kümmerer, D. D. Dionysiou, O. Olsson, D. Fatta-Kassinos, *Science* **2018**, *361*, 222.
[2] A. Mukherji, *Nature* **2022**, *605*, 195.
[3] J. J. Urban, *Joule* **2017**, *1*, 665.
[4] B. Van der Bruggen, *Nat. Rev. Chem.* **2021**, *5*, 217.
[5] X. Yang, A. B. Martinson, J. W. Elam, L. Shao, S. B. Darling, *Matter* **2021,** *4*, 3515.
[6] R. P. Lively, D. S. Sholl, *Nat. Mater.* **2017**, *16*, 276.
[7] J. Hennessy, *Nat. Mater.* **2017**, *16*, 280.
[8] J. Shen, Y. Cai, C. Zhang, W. Wei, C. Chen, L. Liu, K. Yang, Y. Ma, Y. Wang, C. C. Tseng, J. H. Fu, X. Dong, J. Li, X. X. Zhang, L. J. Li, J. Jiang, I. Pinnau, V. Tung, Y. Han, *Nat. Mater.* **2022**, *21*, 1183.
[9] Y. Zhang, J. Guo, G. Han, Y.Bai, Q. Ge, J. Ma, C. H. Lau, L. Shao, *Sci. Adv.* **2021**, *7*, eabe8706.
[10] J. Lu, H. Wang, *Matter* **2021**, *4*, 2810.
[11] Y. Hou, X. Hou, *Science* **2021**, *373*, 628.
[12] R. K. Joshi, P. Carbone, F. C. Wang, V. G. Kravets, Y. Su, I. V. Grigorieva, H. A. Wu, A. K. Geim, R. R. Nair, *Science* **2014**, *343*, 752.
[13] L. Ding, Y. Wei, Y. Wang1, H Chen, J. Caro, H. Wang, *Angew. Chem. Int. Ed.* **2017**, *56*, 1825.
[14] Z. P. Smith, B. D. Freeman, *Angew. Chem. Int. Ed.* **2014**, *53*, 10286.
[15] R. R. Nair, H. A. Wu, P. N. Jayaram, I. V. Grigorieva, A. K. Geim, *Science* **2012**, *335*, 442.
[16] Y. Lu, L. Zhang, L. Shen, W. Liu, R. Karnik, S, Zhang, *Proc. Natl. Acad. Sci. U.S.A.* **2021**, *118*, e2111360118.
[17] Y. Qian, J. Shang, D. Liu, G. Yang, X. Wang, C. Chen, L. Kou, W. Lei, *J. Am. Chem. Soc.* **2021**, *143*, 5080.
[18] Z. J. Fu, S. K. Jiang, X. Y. Chao, C. X. Zhang, Q. Shi, Z. Y. Wang, M. L. Liu, S. P. Sun, *Water Res.* **2022**, *222*, 118888.
[19] S. Zheng, Q. Tu, J. J. Urban, S. Li, B. Mi, *ACS Nano* **2017**, *11*, 6440.
[20] B. Mi, *Science* **2014**, *343*, 740.
[21] C. N. Yeh, K. Raidongia, J. Shao, Q. H. Yang, J. Huang, *Nat. Chem.* **2015**, *7*, 166.
[22] H. Huang, H. Park, J. Huang, *Chem* **2022**, *8*, 2432.
[23] H. Liu, H. Wang, X. Zhang, *Adv. Mater.* **2015**, *27*, 249.
[24] M. Zhang, Y. Mao, G. Liu, G. Liu, Y. Fan, W. Jin, *Angew. Chem. Int. Ed.* **2020**, *132*, 1706.
[25] J. Zhan, Z. Lei, Y. Zhang, *Chem* **2022**, *8*, 947.
[26] L. Chen, G. Shi, J. Shen, B. Peng, B. Zhang, Y. Wang, F. Bian, J. Wang, D. Li, Z. Qian, G. Xu, G. Liu, J. Zeng, L. Zhang, Y. Yang, G. Zhou, M. Wu, W. Jin, J. Li H. Fang, *Nature* **2017**, *550*, 380.
[27] J. Abraham, K. S. Vasu, C. D. Williams, K. Gopinadhan, Y. Su, C. T. Cherian, J. Dix, E. Prestat, S. J. Haigh, I. V. Grigorieva, P. Carbone, A. K. Geim, R. R. Nair, *Nat. Nanotechnol.* **2017**, *12*, 546.
[28] P. Sun, K. Wang, H. Zhu, *Adv. Mater.* **2016**, *28*, 2287.
[29] Y. Zhang, S. Zhang, T. S. Chung, *Environ. Sci. Technol.* **2015**, *49*, 10235.
[30] V. Saraswat, R. M. Jacobberger, J. S. Ostrander, C. L. Hummell, A. J. Way, J. Wang, M. T. Zanni, M. S. Arnold, *ACS Nano* **2018**, *12*, 7855.
[31] C. A. Amadei, A. Montessori, J. P. Kadow, S. Succi, C. D. Vecitis, *Environ. Sci. Technol.* **2017**, *51*, 4280.
[32] X. Chen, S. Mohammed, G. Yang, T. Qian, Y. Chen, H. Ma, Z. Xie, X. Zhang, G. P. Simon, H. Wang, *Adv. Mater.* **2020**, *32*, 2002320.
[33] L. Cheng, Y. Guo, Q. Liu, G. Liu, R. Li, X. Chen, H. Zeng, G. Liu, W. Jin, *Adv. Mater.* **2022**, *34*, 2206349.
[34] Q. Lan, L. Liu, Y. Wu, C. Feng, K. Ou, Z. Wang, Y. Huang, Y. Lv, Y. E. Miao, T. Liu, *Compos. Commun.* **2022**, *33*, 101216.
[35] Z. Tan, S. Chen, X. Peng, L. Zhang, C. Gao, *Science* **2018**, *360*, 518.
[36] L. Jin, Z. Wang, S. Zheng, B. Mi, *J. Membr. Sci.* **2018**, *545*, 11.
[37] Y. Liang, Y. Zhu, C. Liu, K. R. Lee, W. S. Hung, Z. Wang, M. Elimelech, J. Jin, S. Lin, *Nat. Commun.* **2020**, *11*, 2015.
[38] C. L. Ritt, J. R. Werber, M. Wang, Z. Yang, Y. Zhao, H. J. Kulik, M. Elimelech, *Proc. Natl. Acad. Sci.* **2020**, *117*, 30191.
[39] Y. Lv, J. Xia, Y. Yang, Y. Chen, T. Liu, *Compos. Commun.* **2021**, 24, 100695.
[40] R. Sun, Y. Lv, X. Zhang, J. Zhao, Z. Qian, Q. Lan, Z. Wang, T. Liu, *J. Membr. Sci.* **2023**, *672*, 121476.
[41] Q. Yang, Y. Su, C. Chi, K. Huang, V. G. Kravets, F. C. Wang, J. C. Zhang, A. Pratt, A. N. Grigorenko, F. Guinea, A. K. Geim, R. R. Nair, *Nat. Mater.* **2017**, *16*, 1198.
[42] X. Cheng, Y. Qin, Y. Ye, X. Chen, K. Wang, Y. Zhang, A. Figoli, E. Drioli, *Chem. Eng. J.* **2021**, *417*, 127976.

[43] M. B. M. Y. Ang, C. L. Tang, M. R. De Guzman, H. L. C. Maganto, A. R. Caparanga, S. H. Huang, H. A. Tsai, C. C. Hu, K. R. Lee, J. Y. Lai, *Desalination* **2020**, *481*, 114352.
[44] O. Akin, F. Temelli, *Desalination* **2011**, *278*, 387.
[45] S. Karan, Z. Jiang, A. G. Livingston, *Science* **2015**, *348*, 1347.
[46] Z. Jiang, S. Karan, A. G. Livingston, *Adv. Mater.* **2018**, *30*, 1705973.
[47] Y. Liu, S. Zheng, P. Gu, A. J. Ng, M. Wang, Y. Wei, J. J. Urban, B. Mi, *Carbon* **2020**, *160*, 219.
[48] E. R. Nightingale Jr, *J. Phy. Chem.* **1959**, *63*, 1381.
[49] J. Y. Chong, B. Wang, C. Mattevi, K. Li, *J. Membr. Sci.* **2018**, *549*, 385.
[50] S. Kim, X. Lin, R. Ou, H. Liu, X. Zhang, G. P. Simon, C. D. Easton, H. Wang, *J. Mater. Chem. A* **2017**, *5*, 1533.

Entry for the Table of Contents

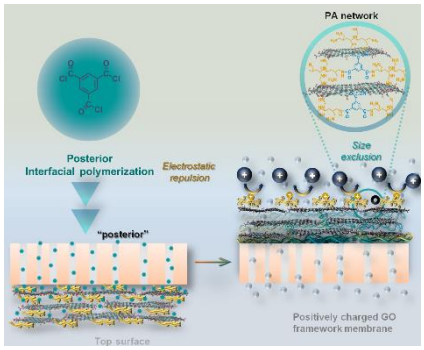

A de novo “posterior” interfacial polymerization strategy is developed to fabricate a highly surface positively charged GO framework membrane for ion sieving. The generated electrostatic repulsion toward ions from the positively charged surface, in conjunction with reinforced size exclusion from the p-IP-formed PA network, endows the membrane with outstanding performance toward ion separation.